J. Phys.: Condens. Matter **11** (1999) 6413–6426. Printed in the UK PII: S0953-8984(99)03371-8

Pattern formation under bistable electro-optical absorption in quantum wells: II

L L Bonilla†, V A Kochelap†‡ and C A Velasco†§

† Universidad Carlos III de Madrid, Escuela Politécnica Superior, Avenida Universidad 30, E-28911 Leganés, Spain

‡ Department of Theoretical Physics, Institute of Semiconductor Physics, National Academy of Sciences, Kiev 252650, Ukraine

Received 13 April 1999

Abstract. In the first part of this work (Bonilla L L, Kochelap V A and Velasco C A 1999 *J. Phys.: Condens. Matter* **11** 6395) we formulated and analysed a model of transverse self-sustained pattern formation in a photoexcited and voltage-biased quantum well (QW) structure. Our model explained the formation of patterns of quasi-neutral two-dimensional electron–hole plasma whose intrinsic bistability was shown in recent experiments. We found patterns containing regions with different spreading of the electron and hole wave functions and different densities of the two-dimensional electron–hole plasma.

In this second part we extend our results to QWs with finite transverse dimension. We will show that the boundary conditions at the edges of the QW layer control the behaviour of the patterns. We will study the stability of the patterns and will show its strong dependence on the boundary conditions. A linear stability criterion for these patterns is presented and compared with numerical simulations.

1. Patterns in quantum wells with finite transverse dimensions

The goal of this part of the work is to discuss the formation of patterns under bistable electro-optical absorption in quantum well (QW) layers of finite transverse dimensions. The details of the model under consideration are given in sections 1 and 2 of the first part of this work [1]. For the sake of completeness, we will briefly review in this section the basic details of our approach.

Our model explains the appearance of quasi-neutral plasma domains in a photoexcited and voltage-biased QW [1–4]. The geometry of the problem consists of a single GaAs QW of width $2d$ subject to a constant electric field due to uniformly distributed charges of a parallel-plate capacitor. The distance between the capacitor plates is $2d_c$, such that $d \ll d_c$, and the field is parallel to the direction of vertical growth of the sample. Furthermore, a monochromatic photon source photoexcites the QW (see figure 1 in [1]).

The approach is based upon the consideration of the widely separated characteristic length scales which are involved in the problem. As detailed in reference [1], we considered in our problem the Schrödinger–Poisson system and the drift–diffusion equations, which we

§ Author to whom any correspondence should be addressed.

0953-8984/99/336413+14$30.00

solved to the leading-order approximation. The resulting second-order equation for the plasma concentration has the expression

$$\frac{\partial n}{\partial \tau} - \frac{\partial}{\partial \xi}\left\{\mathcal{D}(n,q)\frac{\partial n}{\partial \xi}\right\} = a(n,q,\omega)i - n \equiv R(n,q,\omega,i) \tag{1}$$

where all the variables are dimensionless: n is the 2D plasma concentration, τ represents time, ξ is the transverse coordinate, q is the external electric field, $\mathcal{D}$ is a 'diffusion-like' coefficient, a function of the plasma concentration n and the electric field q, and a is the absorption factor. We have assumed that the patterns depend on only one of the transverse coordinates, ξ. $\mathcal{D}$ has the following expression:

$$\mathcal{D}(n,q) \equiv \alpha(n) + n\frac{\partial \epsilon(n,q)}{\partial n} \tag{2}$$

where $\alpha(n)$ is found through the Einstein relation, and ϵ is the lowest two-dimensional subband energy. At the edges of the QW layer we impose these boundary conditions:

$$j_n = -\mathcal{D}(n,q)\frac{\partial n}{\partial \xi} = \pm s^{(\pm)} n \tag{3}$$

where s is the dimensionless edge recombination rate, and the signs $\pm$ correspond to the right and left edges of the QW layer, respectively.

1.1. Stationary states: phase portrait analysis

In section 3 of reference [1], we studied in detail the phase portraits for the stationary solutions of equation (1). Due to the intrinsic bistability of the right-hand side of (1), there are three critical values of the intensity i, i_l, i_k, and i_h, with different phase portraits. In any case, there are three singular points, which we will denote as $n^* = n_1, n_2, n_3$. It was shown that n_1 and n_3 are saddle points, and that n_2 is a centre.

Figure 1 shows these three typical cases. The critical value i_k, found through equation (43) of [1], divides the interval $[i_l, i_h]$ (on which $n(i)$ is multivalued) into two subintervals, $[i_l, i_k)$ and $(i_k, i_h]$. On each subinterval the phase portrait is similar: one of the saddles has a homoclinic orbit enclosing the centre. When $i \in (i_l, i_k)$, the homoclinic orbit belongs to $(n_3, 0)$ as shown in figure 1(a), whereas it belongs to $(n_1, 0)$ when $i \in (i_k, i_h)$ (see figure 1(c)). The phase portrait for $i = i_k$ is shown in figure 1(b).

Let us consider now the case when the transverse extent of the QW layer is finite, $L < \infty$, and the boundary conditions are given by (3). As an example, the boundary curves (3) are marked on the phase plane of figure 1 for several recombination rates. Admissible stationary solutions are trajectories which start on a boundary curve on the positive side of the k-axis and end on a curve on the negative side of the same axis after a 'time of flight' L:

$$\int_{n^{(-)}}^{n^{(+)}} \frac{\mathrm{d}n}{n_\xi(n)} = L \tag{4}$$

where (n, n_ξ) ($n_\xi = \mathrm{d}n/\mathrm{d}\xi$) is an orbit of equation (41) of reference [1] given by an appropriate value of C_1 and $n^{(\pm)} \equiv n(\pm\frac{1}{2}L)$. Let us now consider a few particular cases.

First of all, assume that there is no edge recombination ($s^\pm = 0$). Then the boundary curves coincide with the n-axis. We conclude that all three uniform solutions, n_1, n_2, and n_3, satisfy the boundary conditions, but no open trajectories do. A certain number Q of half-periods of a close trajectory may constitute an eligible solution of the stationary boundary value problem. The spatial period $\xi_p(C_1)$ is a monotonic function of C_1 having a minimum at $C_1 = U(n_2)$ (small-amplitude oscillations around n_2; see equation (40) of reference [1]).

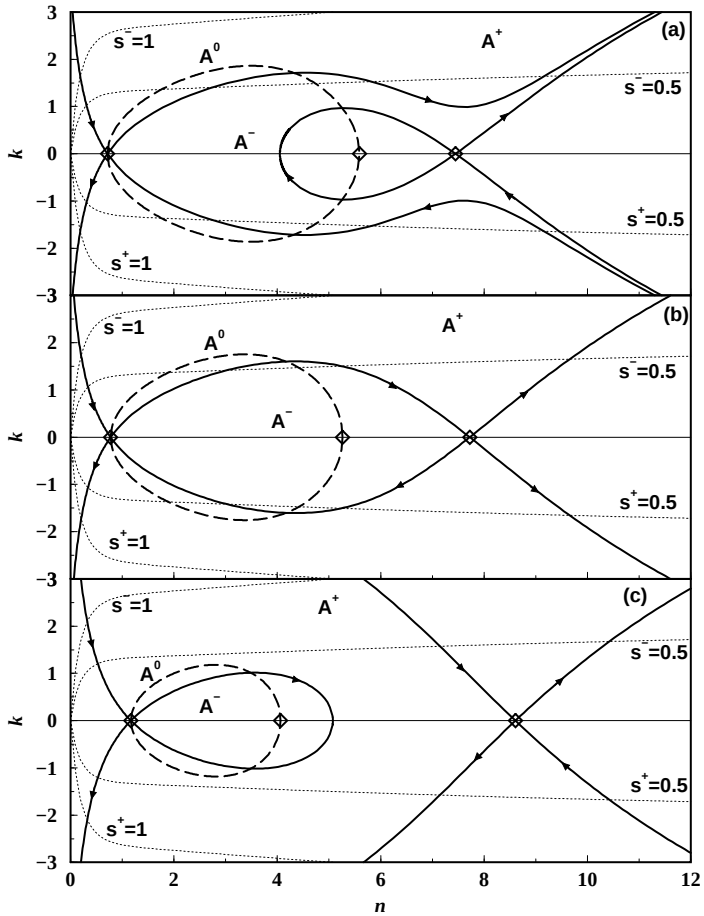

Figure 1. Phase portraits for $i_l < i < i_k$ (a), $i = i_k$ (b), and $i_k < i < i_h$ (c). The solid curves are the separatrices; no other trajectories are portrayed. Diamonds represent the singular points $(n_1, 0)$, $(n_2, 0)$, and $(n_3, 0)$. Dotted curves represent an example of typical symmetric boundary conditions for $s^{\pm} = 0.5$ and $s^{\pm} = 1$. Dashed curves represent the region of the phase plane where we have A^0-type boundary conditions; A^--type boundary conditions apply inside that curve plus the n-axis; A^+-type boundary conditions apply outside of that curve.

When $C_1 \to 0$ (for $i \in [i_l, i_k)$), or $C_1 \to U(n_3)$ (for $i \in (i_k, i_h]$), the period becomes infinite. Admissible trajectories correspond to Q half-periods of a closed orbit with a value of the first integral C_1 such that

$$L = \frac{1}{2} Q \xi_p(C_1). \tag{5}$$

When $L < \frac{1}{2} \min \xi_p$, no suitable trajectories and therefore no nonuniform patterns exist. After $L \geqslant \frac{1}{2} \min \xi_p$, two patterns appear (their amplitude is small if $L \sim \xi_p/2$ and it increases with L; each pattern is transformed into the other by the change $\xi \to -\xi$). These patterns may be called 'half-period' patterns. As $L \gg \min \xi_p$, the width of the nonuniform region in these patterns increases. For $i \in [i_l, i_k)$, the patterns each consist of a plateau with $n = n_3$ which extends almost throughout the sample starting from one of the edges plus a narrow carrier-depleted domain near the other edge (figures 2(a), 2(b)). For $i = i_k$ the patterns may

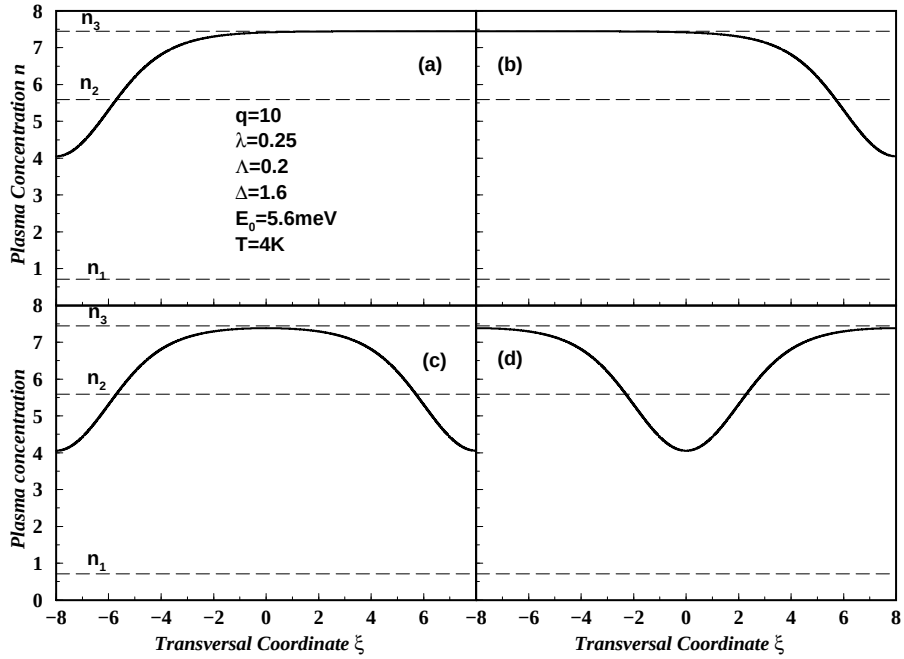

Figure 2. The simplest patterns for $i \in [i_l, i_k)$ and $L > \min \xi_p$ assuming no edge recombination ($s^{\pm} = 0$). (a) and (b) correspond to 'half-period' solutions; (c) and (d) correspond to 'full-period' solutions.

consist of regions of low and high plasma concentration spatially separated by a kink-like transition. For $i \in (i_k, i_h]$, there are extended plateaus of low-concentration plasma and a narrow high-concentration domain near the edge. When $L \geqslant \min \xi_p$, two new solutions of equation (5) arise. They correspond to 'full-period' patterns symmetric with respect to $\xi \to -\xi$. If $i \in [i_l, i_k)$, for example, one pattern consists of a plateau with $n = n_3$ limiting the domains of depleted electron density at both edges (figures 2(c), 2(d)). If $i = i_k$ the patterns consist of three plateaus ($n_3 - n_1 - n_3$, or $n_1 - n_3 - n_1$) separated by proper kink-like transitions. Similar considerations allow us to construct easily the patterns for any other cases.

Let us now consider the case of finite edge recombination, which we analyse for the example of figure 1(a) with $i \in (i_l, i_k]$. This figure shows that uniform patterns are no longer admissible solutions of the boundary value stationary problem. Although patterns with low plasma concentration exist for any recombination velocity $s^{\pm}$, occurrence of patterns with high plasma concentration depends strongly on $s^{\pm}$. When $s^{\pm}$ is small, patterns similar to all those discussed above for $s^{\pm} = 0$ do exist. (We should add appropriate boundary layers near the edges to the patterns of figure 2.) Now let $s_c(i)$ be the edge recombination velocity for which the boundary curve is tangent to the homoclinic orbit in figure 1(a) at a point $(n_c, n_\xi(n_c))$. It is easily found that

$$\begin{aligned} s_c(i) &= \frac{1}{n_c}\sqrt{2\,[U(n_3, i) - U(n_c, i)]} \\ U(n_3, i) &- U(n_c, i) + \frac{n_c}{2} R(n_c)\mathcal{D}(n_c) = 0. \end{aligned} \tag{6}$$

Then, if either of s^+, s^- exceeds $s_c(i)$, no trajectories reaching the high-concentration state satisfy the boundary conditions. Thus no patterns with high-plasma-concentration regions

(either plateaus or narrow domains) exist: there are only simple low-plasma-concentration patterns. Similar conclusions can be reached if $i = i_k$. When $i \in (i_k, i_h]$, some open trajectories are admissible stationary solutions in addition to patterns similar to those previously discussed. As a result, even for $s^{\pm} \to \infty$, these open trajectories provide plateau-like and domain-like patterns with high plasma concentrations (see figure 3).

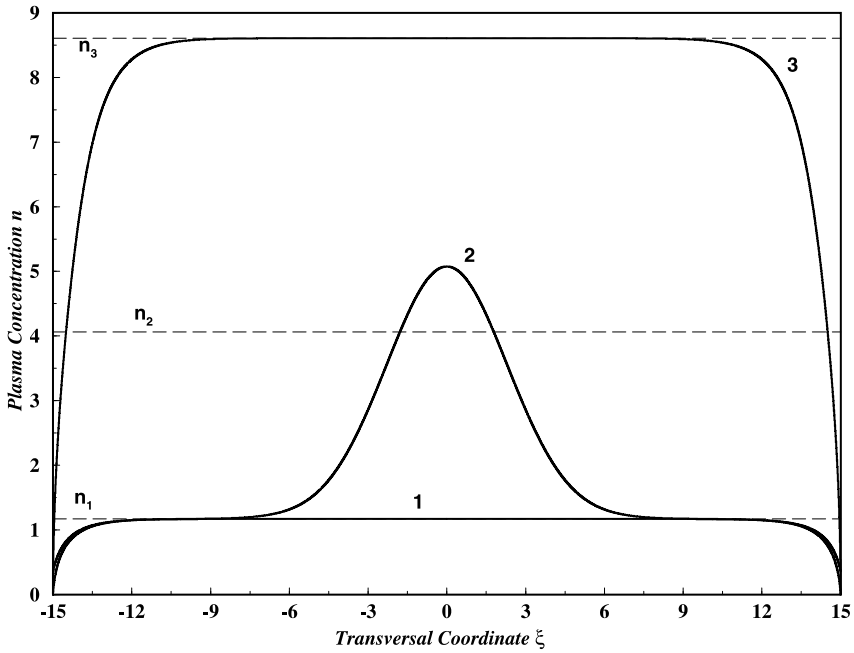

Figure 3. Typical stationary patterns in the range $i_k < i < i_h$ for infinite recombination rates at the edges of the QW layer. Curves (1) and (3) represent stable 'plateau-like' solutions, whereas curve (2) represents an unstable 'domain-like' solution.

The patterns in figure 2 and figure 3 correspond to symmetric boundary conditions $s^+ = s^-$. Trivial modifications of the above considerations allow us to understand how nonsymmetric conditions transform the patterns or even cancel some of them.

2. Stability of a transversely finite QW

In this section we shall characterize the previously constructed transverse patterns in a finite QW according to their linear stability. A general theorem, proven in reference [5], can be used to ascertain the stability of a transverse pattern given its shape and the type of boundary conditions which hold at the edges. This result is summarized in the appendix. The stability analysis of the patterns on a transversely infinite QW can be done in a similar way to other 'infinite patterns' found in the literature. This analysis shows that 'kink-like' structures (corresponding to heteroclinic orbits on the phase plane) are stable, whereas the 'domain-like' structures (corresponding to homoclinic orbits on the phase plane) are unstable. Let us consider a QW layer whose transverse dimension has a finite extent L (left boundary at $\xi = -L/2$ and right boundary at $\xi = L/2$). It is obvious that the stability of a pattern depends on the boundary conditions at the edges of the layer.

2.1. Classification of the boundary conditions

Following the method outlined in the appendix, we define the following functions ($k \equiv \mathrm{d}n/\mathrm{d}\xi$):

$$B_{0,1} \equiv \mathcal{D}(n)\, k \pm s^{\pm} n = 0 \tag{7}$$

where 0 (1) corresponds to $\xi = -L/2$ ($\xi = L/2$). Let us denote by N a solution of the stationary version of equation (1). Then, we find

$$a_0(N) \equiv B_{0p} = \mathcal{D}(n) \qquad \text{at } n(-L/2) \tag{8}$$

$$a_1(N) \equiv B_{1p} = \mathcal{D}(n) \qquad \text{at } n(L/2) \tag{9}$$

$$b_0(N) \equiv B_{0n} = \mathcal{D}'(n)\, k - s^{-} \qquad \text{at } n(-L/2) \qquad n_\xi(-L/2) = k(-L/2) \tag{10}$$

$$b_1(N) \equiv B_{1n} = \mathcal{D}'(n)\, k + s^{+} \qquad \text{at } n(L/2) \qquad n_\xi(L/2) = k(L/2). \tag{11}$$

As the diffusion coefficient $\mathcal{D}(n)$ is strictly positive for $n \geqslant 0$, the boundary conditions have the following properties:

$$n_\xi(\pm L/2) \neq 0 \qquad \text{if } s^{\pm} \neq 0$$

$$n_\xi(\pm L/2) = 0 \qquad \text{otherwise.}$$

Reference [5] (see the appendix) classifies boundary conditions into three types, A^-, A^0, and A^+, according to the sign of an auxiliary function $\Pi_{0,1}$ at each transverse edge of the QW. We compare (at the edges) the slopes of two curves in the phase plane (n, k): the curve defined by the boundary condition and the curve $k(n)$ corresponding to the stationary transverse pattern itself. When the boundary curve is above, tangent to, or below the solution curve, we say that the boundary condition is of type A^+, A^0, or A^-, respectively. See figure 4 for an example. The auxiliary functions Π_i, $i = 0, 1$, provide an analytical characterization of the type of boundary condition. A complete characterization of the linear stability of a steady state according to its shape and the type of boundary condition at the edges was obtained in reference [5].

(a) $s^- = 0$, *and/or* $s^+ = 0$. In this case, $n_\xi(\pm L/2) = 0$, and therefore the *boundary conditions are of type* A^-.

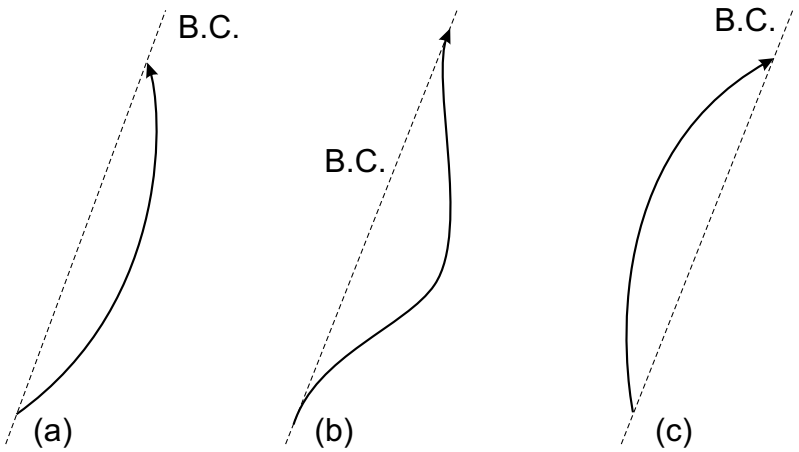

Figure 4. Three examples of boundary conditions of the same type at both edges. The boundary curve is the same straight line at both transverse edges, which lies (a) above (type A^+), (b) tangent to (type A^0), and (c) below the solution curve (type A^-). The arrows on the solution curves mark the direction from $x = 0$ to $x = L$.

(b) $s^{\pm} \neq 0$. Here we define the following terms ($n_\xi(-L/2) > 0$ and $n_\xi(L/2) < 0$):

$$\begin{aligned}\Pi_0 &\equiv -\mathcal{D}[n(-L/2)]n_\xi(-L/2)\{\mathcal{D}[n(-L/2)]n_{\xi\xi}(-L/2) \\ &\quad + [\mathcal{D}'[n(-L/2)]n_\xi(-L/2) - s^-]n_\xi(-L/2)\} \\ &= \mathcal{D}[n(-L/2)]n_\xi(-L/2)\{R[n(-L/2)] + s^- n_\xi(-L/2)\} \qquad (12)\end{aligned}$$

$$\begin{aligned}\Pi_1 &\equiv \mathcal{D}[n(L/2)]n_\xi(L/2)\{\mathcal{D}[n(L/2)]n_{\xi\xi}(L/2) \\ &\quad + [\mathcal{D}'[n(L/2)]n_\xi(L/2) + s^+]n_\xi(L/2)\} \\ &= -\mathcal{D}[n(L/2)]n_\xi(L/2)\{R[n(L/2)] - s^+ n_\xi(L/2)\} \qquad (13)\end{aligned}$$

where we have used the equality $R(n) = -\{\mathcal{D}'(n)n_\xi^2 + \mathcal{D}(n)n_{\xi\xi}\}$. Both terms may be rewritten as follows:

$$\Pi_{0,1} = \mathcal{D}[n(\pm L/2)]|n_\xi(\pm L/2)|\left\{R[n(\pm L/2)] + \mathcal{D}[n(\pm L/2)]\frac{n_\xi^2(\pm L/2)}{n(\pm L/2)}\right\}. \qquad (14)$$

By using (14), we can now determine the regions in space where we have A^--, A^0-, or A^+-type boundary conditions. When

$$R(n) + \mathcal{D}(n)\frac{n_\xi^2}{n} = 0 \qquad (15)$$

we have A^0-type ones, i.e. the region for A^- is the region enclosed between the curves:

$$k(n) \equiv n_\xi = \pm\sqrt{\frac{-R(n)n}{\mathcal{D}(n)}} \qquad n_1 < n < n_2 \qquad (16)$$

and the axis $k = 0$. Notice that the axis $k = 0$ itself is of type A^- as well. $n_1 < n < n_2$ is the region where $R(n) < 0$. These regions are plotted in the phase portraits of figure 1.

2.2. Discussion of stability results

Once the types of the boundary conditions are established, the stability of a given pattern can be determined by finding the sign of the largest eigenvalue (λ_1) of the linearized problem (see the appendix). Let χ, X, and Y be the number of critical points of the stationary solution in the interval $(-L/2, L/2)$, and the type of the left and right boundary conditions, respectively. We have obtained the following results:

(a) *Symmetric patterns.* Under this heading we include cases with no edge recombination ($s^{\pm} = 0$), or with nonvanishing edge recombination ($s^{\pm} \neq 0$). The first ones are like those of figure 2, and the latter are depicted in figure 3 for $s^{\pm} = \infty$.

1. No edge recombination. For this case $X = Y = A^-$, and $\chi = 1$ or $\chi = 0$. Then, according to case 3 of the theorem stated in the appendix, $\lambda_1 > 0$, and therefore, the solutions are *unstable*.
2. Infinite edge recombination. For this case $X = Y = A^+$, and $\chi = 1$. Then, according to case 4 of the theorem stated in the appendix,
$$\mathrm{sgn}(\lambda_1) = -\mathrm{sgn}(n_\xi(-L/2)L_\mu) = -\mathrm{sgn}(L_\mu).$$
Since we have Dirichlet's boundary conditions, L_μ is defined as
$$L_\mu = \frac{\partial L}{\partial n_\xi(-L/2)}.$$
Figure 5 plots the bifurcation diagram for curves similar to (1), (2), and (3) of figure 3. Notice that curves of types (1) and (3) (low- and high-concentration plateaus, respectively) are *stable*, whereas domain-like curves (2) are *unstable*.

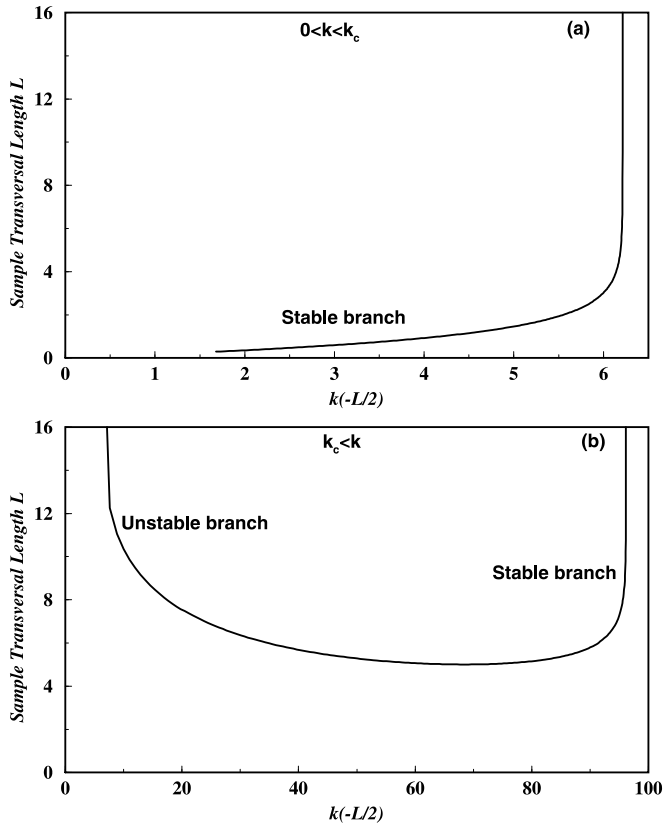

Figure 5. Bifurcation diagrams in the range $i_k < i < i_h$ for infinite recombination rate at the edges of the QW layer. (a) corresponds to $0 < k < k_c$ (curve (1) of figure 3), and (b) corresponds to $k_c < k$ (curves (2), (3) of figure 3). At $k = k_c > 0$, the separatrix entering the saddle $(n_1, 0)$ from the left intersects the k-axis. Positive slope in the bifurcation diagram implies linear stability of the corresponding pattern.

3. Finite edge recombination. The analysis is equivalent to the previous case, but the definition of L_μ changes to
$$L_\mu = \frac{\partial L}{\partial n(-L/2)}.$$
However, the bifurcation diagram is quite similar to that of figure 5.

(b) *Asymmetric patterns.* This paragraph covers a whole variety of cases. As an example, we will consider only asymmetric patterns similar to curves (1), (2), and (3) of figure 3, selecting only half of them. Then we obtain:

1. $X = A^+$, $Y = A^-$ ($s^- = \infty$ and $s^+ = 0$), and $\chi = 0$. We apply case (d) of the theorem stated in the appendix, which coincides with case 2 of the previous paragraph. Those results are thus extensible to this case.
2. $X = A^-$, $Y = A^+$ ($s^- = 0$ and $s^+ = \infty$), and $\chi = 0$. Here we apply case (e) of the theorem stated in the appendix. This implies that
$$\mathrm{sgn}(\lambda_1) = \mathrm{sgn}(n_\xi(L/2)L_\mu) = -\mathrm{sgn}(L_\mu).$$
And L_μ is defined as in case 3 of the previous paragraph, and the results are applicable here.

Notice how a simple method like the one stated in the appendix, together with the help of the phase portraits of figure 1, can give us an immediate result about the stability of the patterns. In general terms, it can be said that the recombination rate has a stabilizing effect. However, when $i \in (i_l, i_k)$, a high recombination rate cancels many possible patterns. The stability results were checked by studying the dynamics of (1) with a standard moving-grid numerical method to integrate parabolic differential equations [6]. We started by choosing an appropriate initial density profile and then observing its evolution towards a stable pattern (whose stability had been established by using the previous criteria). For the first case (figure 3, curve (1)), we chose $n(\xi, 0)$ as a parabola whose maximum was smaller than n_1. This profile evolved towards our first solution (see figure 6(a)). Any small disturbance of the final state would lead again to that solution. As regards the pattern with the high plateau (figure 3, curve (3)), we chose as initial profile a parabola with a maximum larger than the maximum of the second (unstable) stationary solution (see figure 3, curve (2)). The initial profile evolved towards the third

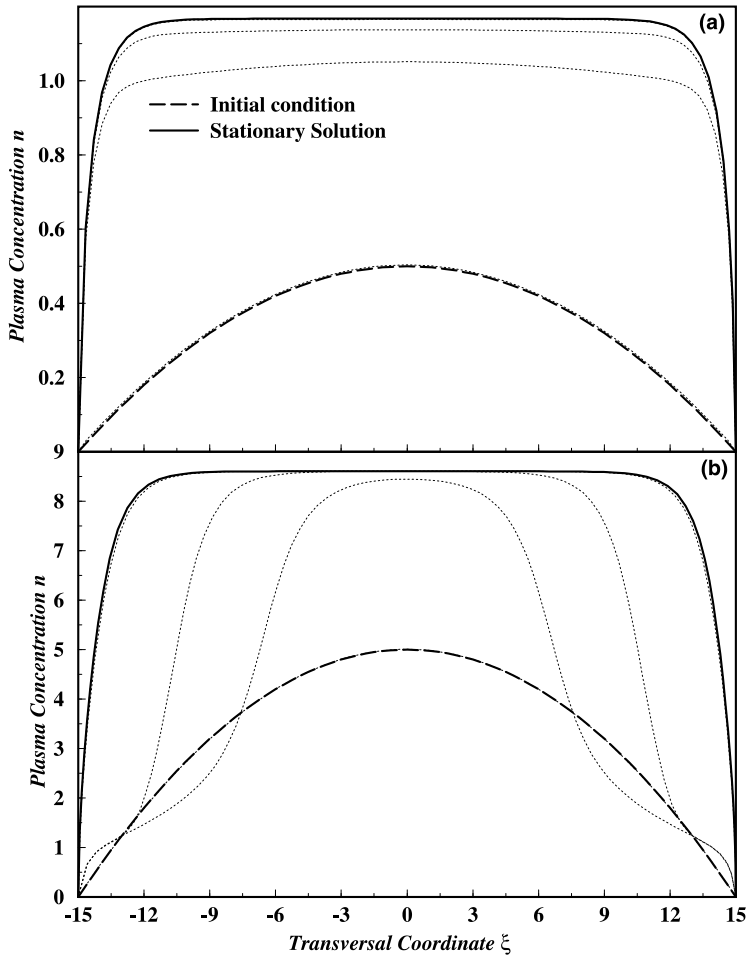

Figure 6. Evolution towards a stable stationary solution (solid curve) in the QW layer from an initial profile. Dotted curves are profiles at intermediate times. (a) corresponds to curve (1) and (b) corresponds to curve (3) of figure 3.

stationary solution (see figure 6(b)). However, in the intermediate case (figure 3, curve (2)), when we analysed a small disturbance of the stationary solution (step-like or sinusoidal), the system departed rapidly from the unstable pattern (see figure 7).

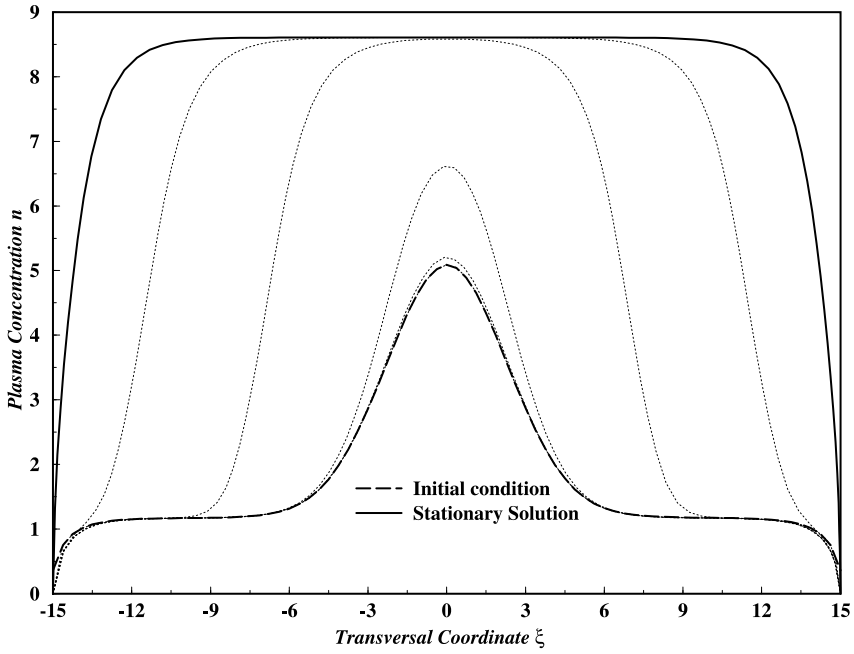

Figure 7. As figure 6, but starting from an initial profile very close to an unstable stationary solution (curve (2) in figure 3) in the QW layer.

3. Discussion

We shall present an overall discussion of the results of parts I and II of this work. We have formulated and analysed a model of pattern formation in a QW heterostructure under bistable electro-optical absorption. The model includes: self-consistent calculations of the wave functions and subband energies of the photoexcited electrons and holes in an strongly biased QW, nonlinear interband light absorption, the configuration of the electrostatic potential, its screening, and the transverse motion of the two-dimensional electron–hole plasma. The quantized vertical motion and the semiclassical transverse motion of the carriers are *strongly coupled* due to the electrostatic interaction. The transverse redistribution of the carriers induces the electrostatic mean-field potential, and adiabatically drives the electron and hole wave functions, and the subband energies. In the numerical calculations we used values taken from experiments [2–4], and the literature. Thus our maximum concentrations are in the range of those measured in the experiments, $3\text{–}5\times10^{11}\,\mathrm{cm}^{-2}$, for a typical electric field $\mathcal{E}\sim 60\,\mathrm{kV\,cm}^{-1}$.

The analysis of this model has shown that a variety of stationary patterns are possible. The characteristic scale of the transverse plasma redistribution is the ambipolar diffusion length $L_{\mathcal{D}}$. When the transverse dimension is very large, the patterns consist of extended plateaus with high (low) plasma concentration and layers of low (high) plasma concentration outside the plateaus. The electron and hole wave functions are redistributed within the QW layer, i.e., they vary on the well thickness scale d. At some specific intensity, the plateaus with low and

high plasma density can coexist. They are separated by a kink-like transient region whose width is also of the order of $L_{\mathcal{D}}$.

For a QW layer of finite transverse extent, some possible patterns are selected by the transverse dimensions of the layer and the boundary conditions at the edges. A large electron–hole recombination at the edges diminishes the number of possible patterns, and may cancel the bistable or multistable behaviour of the patterns for a whole range of external parameters. Notice that different patterns in the QW layer induce different potential distributions outside this layer, as shown in figure 6 of reference [1] for the example of the antisoliton solution of figure 4(a) of the same paper.

As expected, the stability of the patterns depends strongly on the boundary conditions. From our results, it can be concluded that the recombination rate has a stabilizing effect on the patterns, with the already mentioned effect of cancellation of patterns in some range of light intensities ($i \in (i_l, i_k)$).

An interesting phenomenon was found in the analysis of QWs with finite transverse dimensions when applying *asymmetric boundary conditions* to the layer. These conditions induce a transverse voltage drop which can be calculated with equation (26) of reference [1]. This voltage drop arises due to pattern formation despite the assumed uniform illumination of the QW layer. We can give a numerical estimate for this induced drop in the QW layer when the boundary conditions are strongly asymmetric ($s^- = 0$, $s^+ \gg 1$). When the transverse dimension of the layer is large ($L \gg L_{\mathcal{D}}$), three patterns analogous to those of figure 3 may be realized:

(a) a plateau $n = n_1$ starting from the '$-$' edge and changing to an accumulation layer near the '+' edge;

(b) a high-density layer $n > n_2$ near the '$-$' edge which changes to a plateau $n = n_1$ occupying most of the transverse extent of the QW, and then changes to a depletion layer at the '+' edge;

(c) the plateau $n = n_3$ which is transformed into a depletion layer at the '+' edge.

For these patterns we obtain an induced transverse voltage drop ($L = 15$): $|V_{pl}| = (1/e)E_0(\phi(n^+) - \phi(n^-)) = 4.7$ mV, 11.7 mV, 17.4 mV, respectively. Notice that the total transverse voltage drop is not small in spite of the smallness of the induced transverse electric fields. In the examples studied, the vertical voltage drop across the QW is $\Delta V = 2dq\mathcal{E}_0 =$ 112 mV, and the maximum transverse drop for the given dimension reaches 15% of the drop across the well. This supports our previous statement about the strong coupling between vertical and transverse effects in these systems.

We conclude by remarking that formation of patterns similar to those described in this work can be found in other cases of reported bistable electro-optical effects in quantum heterostructures [7–13], to which our approach could be extended.

Acknowledgments

We thank Dr V N Sokolov for useful discussions. We are indebted to the Dirección General de Enseñanza Superior (Spanish Ministry of Education) for sabbatical support (VAK) and for financial support through grant PB97-0088, and to the UE Training and Mobility of Researchers Programme through contract ERBFMBXCT970157. One of us (CAV) acknowledges the support of the Fundación General de la Universidad Carlos III de Madrid.

Appendix. Stability criteria

Reference [5] states and proves a simple geometric criterion on the linear stability of stationary solutions of nonlinear second-order parabolic equations on a finite segment. For the sake of completeness, we will summarize this approach in the rest of the appendix. We begin with a generic parabolic operator:

$$f(u, u_x, u_{xx}, u_t) = 0 \qquad \text{in } 0 < x < L,\ t > 0 \tag{A.1}$$

$$\begin{aligned} &B_0(u, u_x) = 0 && \text{at } x = 0 \\ &B_1(u, u_x) = 0 && \text{at } x = L \end{aligned} \tag{A.2}$$

where f, B_0, and B_1 are $\mathcal{C}^1$ functions such that $f_q(u, p, q, r) > 1$, $f_r(u, p, q, r) < -1$ whenever $f(u, p, q, r) = 0$ (i.e., equation (A.1) is uniformly parabolic), and, for $i = 0, 1$, $B_{iu}(u, p)^2 + B_{ip}(u, p)^2 \neq 0$ whenever $B_i(u, p) = 0$ (i.e., the boundary conditions (A.2) define simple curves in the phase plane of (A.1) with $u_t = 0$).

Linear stability properties of a stationary solution of equations (A.1) and (A.2), U, are defined in terms of the sign of the largest eigenvalue, λ_1, of the linearized problem:

$$\begin{aligned} &\mathcal{L}(U)v = \lambda v && \text{in } 0 < x < L \\ &\mathcal{B}_i(U)v = 0 && \text{at } x = iL, \text{ for } i = 0, 1 \end{aligned} \tag{A.3}$$

where the operators $\mathcal{L}(U)$, $\mathcal{B}_0(U)$, and $\mathcal{B}_1(U)$ are defined as

$$\begin{aligned} &\mathcal{L}(U)v \equiv \phi(x)v'' + \varphi(x)v' + \psi(x)v \\ &\mathcal{B}_i(U)v \equiv a_i(U)v' + b_i(U)v \end{aligned} \tag{A.4}$$

where for $x \in (0, L)$, $\phi(x) = -f_q/f_r$, $\varphi(x) = -f_p/f_r$, and $\psi(x) = -f_u/f_r$, at $(u, p, q, r) = (U(x), U_x(x), U_{xx}(x), 0)$, and for $i = 0, 1$,

$$a_i(U) = B_{ip}\ b_i(U) = B_{iu} \qquad \text{at } (u, p) = (U(iL), U_x(iL)). \tag{A.5}$$

As is well known, the eigenvalues of (A.3) are real, and the eigenfunctions associated with λ_1 do not vanish in $0 < x < L$. The stationary solution U is linearly exponentially stable (linearly stable or unstable) if $\lambda_1 < 0$ ($\lambda_1 \leqslant 0$ or $\lambda_1 > 0$).

Reference [5] classifies the boundary conditions (A.2) into three types, A^-, A^0, or A^+, according to whether the boundary curve is below, tangent to, or above the solution curve in the (u, u_x) phase plane; see figure 4. The slopes of the boundary and solution curves are $-a_i(U)/b_i(U)$ and U_{xx}/U_x, respectively. Then it can be shown that the type of boundary condition depends on the sign of

$$\Sigma \equiv (-1)^{i+1} a_i(U)U_x(iL)\,[a_i(U)U_{xx}(iL) + b_i(U)U_x(iL)] \tag{A.6}$$

if $a_i(U) \neq 0$ and $U_x(iL) \neq 0$.

When

$$\Sigma \left\{ \begin{array}{c} < 0 \\ = 0 \\ > 0 \end{array} \right\}$$

the boundary condition (A.2) at $x = iL$ is of type

$$\left\{ \begin{array}{c} A^- \\ A^0 \\ A^+ \end{array} \right\}$$

with respect to the stationary solution U. If $a_i(U) = 0$ and $U_x(iL) = 0$ ($\neq 0$), then the boundary condition (A.2) at $x = iL$ is of type A^0 (A^+). Finally, if $a_i(U) \neq 0$ and $U_x(iL) = 0$,

the boundary condition (A.2) at $x = iL$ is of type A^-. We see that a pure Neumann boundary condition is of type A^-. On the other hand, a pure Dirichlet boundary condition is usually of type A^+, unless U_x happens to be zero, in which case it is of type A^0.

With this classification in mind, reference [5] states the following:

Theorem. Under the above assumptions, let U be a stationary solution of (A.1) and (A.2), let λ_1 be the largest eigenvalue of the linearized problem (A.3), let n be the number of critical points of U in the interval $(0, L)$, and let X and Y ($=A^-$, A^0, or A^+) be the type of the boundary conditions (A.2), at $x = 0$ and $x = L$ respectively, with respect to U. Then,

(a) $\lambda_1 < 0$ if $n = 0$ and either

$$\begin{cases} \text{(i) } X = A^+ \text{ and } Y = A^0 \text{ or } A^+ \text{ or} \\ \text{(ii) } X = A^0 \text{ or } A^+ \text{ and } Y = A^+. \end{cases}$$

(b) $\lambda_1 = 0$ if $n = 0$ and $X = Y = A^0$.

(c) $\lambda_1 > 0$ if either

$$\begin{cases} \text{(i) } n \geqslant 2 \text{ or} \\ \text{(ii) } n = 1 \text{ and either } X \text{ or } Y \text{ is equal to } A^- \text{ or } A^0 \text{ or} \\ \text{(iii) } n = 0,\ X = A^- \text{ and } Y = A^- \text{ or } A^0 \text{ or} \\ \text{(iv) } n = 0,\ X = A^- \text{ or } A^0 \text{ and } Y = A^-. \end{cases}$$

(d) $\operatorname{sgn}(\lambda_1) = -\operatorname{sgn}(U_x(0)L_\mu)$, if either

$$\begin{cases} \text{(i) } n = 1 \text{ and } X = Y = A^+ \text{ or} \\ \text{(ii) } n = 0,\ X = A^+ \text{ and } Y = A^-. \end{cases}$$

(e) $\operatorname{sgn}(\lambda_1) = \operatorname{sgn}(U_x(L)L_\mu)$, if $n = 0$, $X = A^-$ and $Y = A^+$.

Here $\operatorname{sgn}(x) = x/|x|$, if $x \neq 0$, and $\operatorname{sgn}(0) = 0$.

The parameter L_μ may be defined in two ways which are equivalent to the following easily visualized construction:

(a) $a_0[U(0)] \neq 0$. We plot a bifurcation diagram of $u(0)$ versus the segment length L (bifurcation parameter). Then we define $L_\mu = \partial L/\partial u(0)$ calculated at the actual sample length.

(b) $a_0[U(0)] = 0$. We plot a bifurcation diagram of $u_x(0)$ against the segment length L (bifurcation parameter). Then we define $L_\mu = \partial L/\partial u_x(0)$ calculated at the actual sample length. This is the case for typical Dirichlet boundary conditions.

References

[1] Bonilla L L, Kochelap V A and Velasco C A 1999 *J. Phys.: Condens. Matter* **11** 6395

[2] Merlin R 1989 in *Spectroscopy of Semiconductor Microstructures (NATO ASI Series B: Physics, vol 206)* (Dordrecht: Kluwer) p 347

[3] Merlin R, Mestres N, McKiernan A, Oh J and Bhattacharya P K 1990 *Surf. Sci.* **228** 88

[4] Merlin R and Kessler D A 1990 *Phys. Rev.* B **41** 9953

[5] Bonilla L L, Higuera F J and Vega J M 1991 *Appl. Math. Lett.* **4** 41

[6] Sanz-Serna J M and Christie I 1986 *J. Comput. Phys.* **67** 348
Blom J G, Sanz-Serna J M and Verwer J G 1987 *Centre for Mathematics and Computer Science, Amsterdam, Report* NM-R8713
Blom J G, Sanz-Serna J M and Verwer J G 1988 *J. Comput. Phys.* **74** 191
Blom J G, Sanz-Serna J M and Verwer J G 1988 *Centre for Mathematics and Computer Science, Amsterdam, Report* NM-R8804

[7] Bonilla L L, Kochelap V A, Sokolov V N and Velasco C A 1998 *J. Phys. C: Solid State Phys.* **31** L539

[8] Miller D A B, Chemla D S, Damen T C, Wood T H, Burrus C A, Gossard A C and Wiegmann W 1984 *Appl. Phys. Lett.* **45** 13
[9] Miller D A B, Chemla D S, Damen T C, Wood T H, Burrus C A, Gossard A C and Wiegmann W 1985 *IEEE J. Quantum Electron.* **21** 1462
[10] Lentine A L, Hinton H S, Miller D A B, Henry J E, Cunningham J E and Chirovski L M F 1989 *IEEE J. Quantum Electron.* **25** 1928
[11] Miller D A B 1990 *Opt. Quantum Electron.* **22** S-61
[12] Abe Y and Tokuda Y 1993 *Appl. Phys. Lett.* **63** 3259
[13] Couturier J, Voisin P and Harmand J C 1993 *J. Physique Coll.* **3** C5 253
Couturier J, Voisin P and Harmand J C 1994 *Appl. Phys. Lett.* **64** 742
Couturier J, Voisin P and Harmand J C 1995 *Semicond. Sci. Technol.* **10** 881